Ab initio modeling of primary processes in photosynthesis : protein induced activation of bacteriochlorophylls for efficient light harvesting and charge separation

Wawrzyniak, P.K.

Chapter 3

Protein-induced Geometric Constraints and Charge Transfer in BChl *a*–His Complexes of LH2

3.1 Introduction

In this chapter a systematic DFT study of the NMR chemical shifts for histidine and for bacteriochlorophyll *a*–histidine complexes in the light-harvesting complex II is performed. The investigated protonation states of the imidazole side chain include also neutral$_\pi$ and the anionic cases, which, although not much studied in the literature, appear to play an important function in biological systems. Recently it has been argued that the negatively charged histidine may play a role in the electron transfer process in Photosystem II. [79]

The computed chemical shift patterns are consistent with available experimental data for cationic and neutral$_\tau$ crystalline histidines. The results for the bacteriochlorophyll *a*–histidine complexes in LH2 strongly suggest that the protein environment in LH2 exerts a stress on the histidine coordinated to the bacteriochlorophyll *a* resulting in a large charge transfer and a com-

bined structural change. Due to this protein induced geometric constraint, the Mg-coordinated histidine in LH2 appears to be in a frustrated state very different from the formal neutral$_\pi$ form. Finally, the pyridine character of the Mg-bound nitrogen in the LH2 complex is addressed, together with discussion on the effect of hydrogen bonds on the histidine chemical shifts.

The results and discussion section contains first the calculations for histidine in vacuum in comparison with available experimental data for lyophilized crystalline samples of histidine and a discussion on the accuracy of DFT chemical shifts. The following subsections address the problem of protonation state assignment in non-coordinated and Mg-coordinated histidines in LH2.

3.2 Models and Methods

All calculations for His and BChl *a*–His complexes were performed in vacuum within the DFT framework with the Gaussian 03 package. [80] The applied BLYP [73, 75, 76] exchange-correlation functional has been already shown to produce accurate chemical shifts for similar systems. [81] Additionally the B3LYP hybrid functional [75–77] was tested (Table A.2 in the appendix) and it has a marginal effect on the chemical shifts when compared to BLYP.

Basis set tests were performed for the reference compounds (TMS, NH_3) and histidine in all four possible protonation states of its imidazole ring. The discussion is presented in the appendix, together with the results collected in the appendix Tables A.1 and A.3. Based on these tests, the 6-311++G(d,p) basis set was chosen for the remaining part of the study, except for the geometry optimization of the BChl *a*–His complexes (Fig. 3.1) where the 6-31++G(d,p) basis set was used.

The initial structure for the BChl *a*–His complex in LH2 was extracted from one of the B850 BChl dimer units in the 2FKW PDB crystallographic structure of *Rps. acidophila*. [36] According to the crystal structure the two BChl *a* molecules in the dimer are slightly asymmetric, but the two histidines coordinated to them appear to be equivalent according to the NMR spectra. [26, 39] Therefore only one subunit of the dimer was included, namely β-His 30 and BChl 1601, since the characterization of the histidine chemical

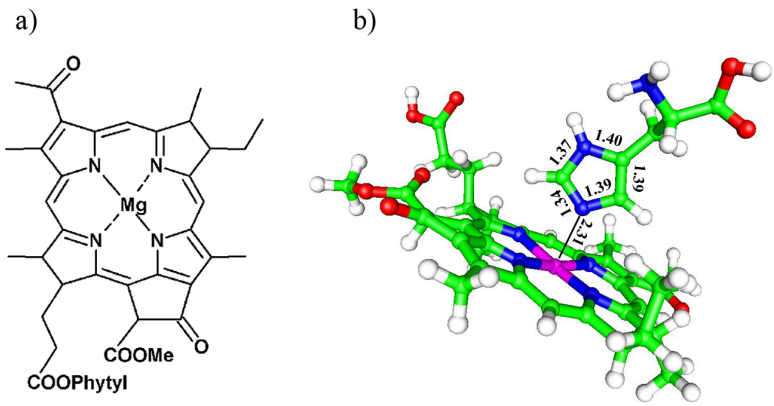

Figure 3.1: a) Schematic representation of the bacteriochlorophyll *a* structure. b) DFT-optimized structure of the neutral BChl *a*–His complex. The phytyl tail was truncated at the esther group and substituted by a hydrogen atom. The bond lengths in the imidazole ring and the Mg–N_τ distance (Å) are also shown.

shifts is the primary aim. To model histidines in a protein environment a neutral amino acid termination (COOH–NH_2) was used to saturate the broken peptide bond. Other protonation states of the amino acid termination that can occur in solution are not of interest for this work. The phytyl tail of the bacteriochlorophyll *a* was truncated at the esther group and saturated by a hydrogen atom in the model (see Fig. 3.1). This truncation does not affect the electronic structure of the porphyrin ring.

The geometries were fully optimized and the NMR chemical shieldings were calculated using the GIAO method. [82–85] The calculated ^{1}H and ^{13}C chemical shieldings were referred to the TMS chemical shifts scale, while the computed ^{15}N chemical shieldings were referred to the value of $^{15}NH_3$. The experimental chemical shifts referred to $(^{15}NH_4)_2SO_4$ powder were converted to the $^{15}NH_3$ scale by adding 20 ppm, as suggested in ref. [86].

The ADF program [87–89] was used to calculate the electron charge difference map between the BChl *a*–His complex and its two fragments, histidine and bacteriochlorophyll *a*. The BLYP functional with the TZP Slater-type basis set was used for this calculation.

3.3 Results and Discussion

3.3.1 Chemical shifts calculations for histidine in vacuum

Geometry

Figure 3.2 shows a comparison of the imidazole ring bond lengths in the DFT-optimized histidine with available crystal structures. Several crystal

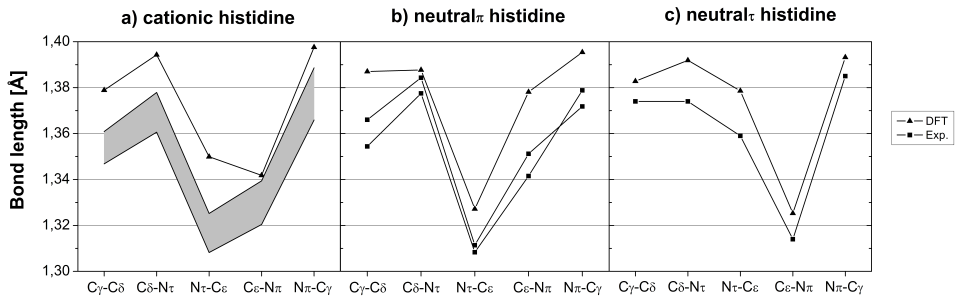

Figure 3.2: Comparison between experimental and DFT bond lengths in the imidazole ring of histidine. a) Cationic histidine. The experimental values are from ref. [21,90,91]. The grey area represents the experimental range of bond lengths from different crystal structures. b) Neutral$_\pi$ and c) neutral$_\tau$ histidines. The experimental values are from ref. [21] and [92], respectively.

structures available in the Cambridge Structural Database were analyzed, namely ADAVOQ [21], ADAVUW [21], CAMWOD [90], CAMWUJ [90], ZOZWAM [91], as well as the structure determined by Edington *et al.* [92]. Interestingly, the ADAVUW structure contains two cationic and two neutral$_\pi$ histidines in the unit cell and, according to our knowledge, it is the only evidence of the neutral$_\pi$ tautomer in a simple crystal compound. A very good agreement in the bond lengths is observed for all the available histidine forms, with only a small systematic overestimation of around 2%. This is a typical DFT accuracy for the geometrical parameters, especially taking into account that the specific crystalline environments are neglected. It is worth pointing out that the optimized geometries of the cationic and neutral$_\pi$ histidines show an intra-molecular hydrogen bond between N$_\pi$ and the C=O group of the histidine tail.

Chemical shifts

Table 3.1 and Figure 3.3 present a comparison of the calculated histidine chemical shifts with NMR measurements on crystal samples [26, 29] available only for histidines with a cationic and neutral$_\tau$ imidazole ring. [29] The com-

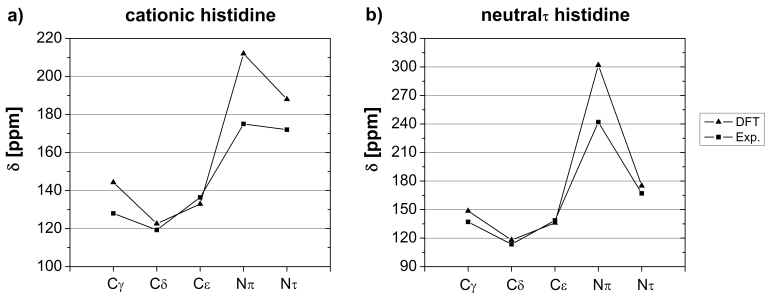

Figure 3.3: Comparison between experimental and DFT chemical shifts [ppm] for a) cationic histidine and b) neutral$_\tau$ histidine. The experimental values are from ref. [26, 29] for histidine crystal samples.

parison shows a good agreement for C_δ and C_ε (≈4 ppm error on average, 3%) and for N_τ (≈12 ppm error on average, 7%). The largest deviations are observed for C_γ (16 ppm, 13%) and N_π (60 ppm, 25%). Unfortunately, for the neutral$_\pi$ tautomer only selected chemical shifts within various protein environments have been reported. [25] However, this tautomer has been already observed in a simple compound [21] and could be used in the future as a generic model for chemical shifts of neutral$_\pi$ histidine. Interestingly, DFT predicts that the three ^{13}C signals in neutral$_\pi$ histidine should appear very close to each other, contrary to the other three forms (Table 3.1). Moreover, the condition mentioned in the introduction to distinguish between the two neutral tautomers [25] is satisfied by the computed C_δ chemical shifts.

A direct comparison for the doubly deprotonated histidine is also not possible as it has never been clearly observed experimentally. According to the calculations the most peculiar feature of the anionic form is the remarkably large C_ε chemical shift value of 154 ppm, which is about 20 ppm downfield compared to the other three cases. This supports the suggestion that a doubly deprotonated histidine may be present in the Photosystem II. [79]

	Histidine (exp.)[a)]		Histidine (DFT)					4-Methylimidazole (DFT)		
	cationic	neutral$_\tau$	cationic	neutral$_\tau$	neutral$_\tau$...x	neutral$_\pi$	anionic	neutral$_\tau$	neutral$_\pi$	neutral$_\pi$...x
C$_\gamma$	128.0	137.0	144.3	148.5	147.7	131.6	137.7	147.3	129.8	130.7
C$_\delta$	119.3	113.5	122.6	117.9	118.0	134.5	133.4	113.9	133.6	133.4
C$_\varepsilon$	136.4	138.6	132.9	136.0	137.1	137.3	154.0	136.3	136.8	137.0
N$_\pi$	175	242	212	302	301	190	293	306	183	192
N$_\tau$	172	167	188	175	186	303	295	174	304	302
H$_\delta$			7.2	6.9	6.9	7.0	7.0	6.7	6.9	6.8
H$_\varepsilon$			8.0	7.4	7.5	7.3	7.4	7.3	7.3	7.4

[a)] ^{13}C chemical shifts from ref. [26], ^{15}N chemical shifts from ref. [29].

Table 3.1: Calculated histidine and 4-methylimidazole chemical shifts [ppm] for different protonation states in comparison with available experimental data for crystal histidine. The experimental values for ^{15}N are converted to NH_3 as a reference compound (see section on computational details). 'x' denotes an inter-molecular hydrogen bond with a water molecule at the pyrrole nitrogen.

Table 3.1 contains also the chemical shifts computed for two neutral tautomers of the 4-methylimidazole. These chemical shifts are very similar to those of neutral histidines, except for N_π in the neutral$_\pi$ tautomer where a difference of 7 ppm is observed. When adding a water molecule forming an inter-molecular hydrogen bond to 4-MeIm at the π position, the N_π chemical shift has almost the same value as in neutral$_\pi$ histidine. This result shows that the inter-molecular and the intra-molecular H-bond have the same effect on the N_π chemical shift. It can be also noticed that the chemical shifts of C_ε are almost equal in the two neutral tautomers due to the symmetry of the ring.

Apart from comparing absolute values, it is also useful to compare the chemical shift changes upon protonation or deprotonation of the imidazole ring. In this way systematic DFT errors are partially canceled and it is easier to identify trends that may help in the assignment of histidine protonation states. Figure 3.4a presents the experimental, denoted as 'Exp. Crystal', and DFT chemical shift differences between cationic and neutral$_\tau$ histidines defined as $\Delta\delta = \delta_{\mathrm{form1}} - \delta_{\mathrm{form2}}$. The pattern in $\Delta\delta$ is correctly reproduced by the calculation. The largest deviations from experiment are found for the N_τ (7.7 ppm) and N_π (23 ppm) nitrogens.

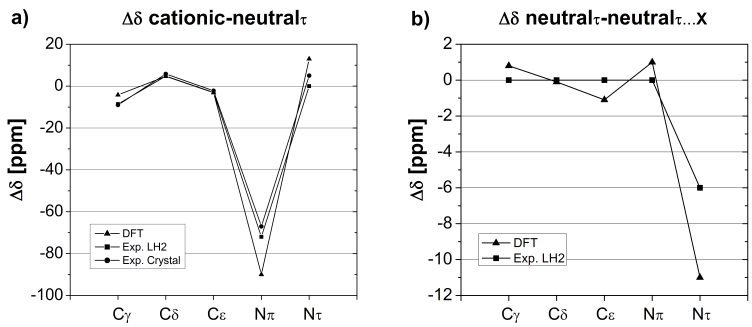

Figure 3.4: a) Chemical shift difference $\Delta\delta = \delta_{\mathrm{cationic}} - \delta_{\mathrm{neutral}\tau}$ [ppm] derived for DFT calculations, histidine crystal samples [26,29] and β-His 41, α-His 37 in LH2 [26,39]. b) Chemical shift difference $\Delta\delta$ [ppm] between neutral$_\tau$ tautomer and neutral$_\tau$ with H-bond on the N_τ atom derived for DFT calculations and α-His 37, β-His 12 in LH2 [26,39].

Source of error for chemical shifts

The comparison between theoretical and experimental chemical shifts exhibits an overall good agreement for the carbon atoms. The largest deviation is observed for C_γ, possibly due to the large effect of the environment on this particular carbon, related to the tail orientation. Indeed C_γ is known to be sensitive to the protein environment and for that reason is not used for discriminating between the two neutral tautomers. [25]

Although the pyrrole and pyridine character of the nitrogens in the different protonation states is correctly reproduced by the calculation, significant differences with the experimental values are observed for ^{15}N chemical shifts. Due to the high polarizability of the nitrogen atom, hydrogen bonding and other intermolecular interactions strongly affect the ^{15}N chemical shieldings. [27, 93–96] By neglecting those effects, the standard deviation between experimental and DFT ^{15}N chemical shifts may be as large as 30 ppm [97], which is 18% of the protonated ^{15}N chemical shift value. Moreover, even if those intermolecular interactions are included, an error of 17 ppm (10%) is still observed. [97] These previous findings are in line with the errors observed in the present calculations. A considerable effort is under way in finding efficient ways of including the environmental effects in the chemical shift calculations through embedding schemes at various levels of accuracy. [98–100] An explicit inclusion of the crystal environment is outside the scope of the present work. In conclusion, some care should be taken when comparing DFT absolute chemical shifts with experimental data, especially for nitrogen atoms. The comparison of relative chemical shifts is more reliable since the error is partially canceled out, as may be seen in Figure 3.4.

3.3.2 Protonation state of histidines in the LH2 complex

Non-coordinated histidines (α-His 37, β-His 12, β-His 41)

Experimentally resolved NMR chemical shifts for histidines in LH2 are shown in Table 3.2. The proposed assignment was based on the experimental values for crystal samples of histidine. [26, 39] It was also suggested, based on the nitrogen chemical shifts, that some of the histidines in LH2 are involved in

	Experiment LH2 [a]				DFT				
	β-His 12	α-His 37	β-His 41	α-His 31, β-His 30	**1**	**2**	**3**	**4**	**5**
	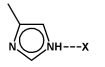		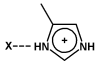	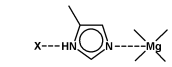	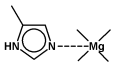	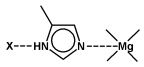	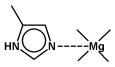	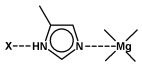	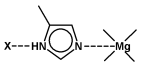
C_γ	133.7	133.7	125.1	125.1	133.6	134.1	129.5	130.0	128.8
C_δ	113.5	113.5	118.3	118.3	129.7	128.6	124.5	123.7	125.2
C_ε	136.5	136.5	133.5	133.5	135.6	136.5	132.2	131.4	134.3
N_π	250	250	178	178	188	196	175	183	196
N_τ	176	170	170	225	277	277	281	278	273
H_δ	6.2	6.2	6.5	2.6	3.0	2.9	4.6	4.4	3.8
H_ε	7.4	7.4	7.9	4.2	3.1	3.2	3.3	3.6	4.7

[a] from ref. [26,39]

Table 3.2: Calculated and experimental chemical shifts for histidines in the LH2 complex. In the schematic representation of the model, the histidine tail and the remaining part of the BChl *a* molecule were omitted for clarity. The indicated charge of histidine is the formal charge. 'X' denotes a hydrogen bond. The structure of the complexes **1** and **2** was fully optimized, the complexes **3** and **4** corresponds to the X-ray structure of LH2 [36], while the complex **5** was partially optimized (see text for details).

hydrogen bond interactions. [26,39] The chemical shift difference $\Delta\delta$ between cationic β-His 41 and the neutral α-His 37 is shown in Figure 3.4a (Exp. LH2) together with the DFT-predicted $\Delta\delta$ between cationic and neutral$_\tau$ histidine in vacuum. The experimental pattern is correctly reproduced: The $\Delta\delta$ for C_γ and C_ε is predicted to be -4.2 ppm ($\Delta\delta^{exp} = -8.6$ ppm) and -3.1 ppm ($\Delta\delta^{exp} = -3.0$ ppm), respectively, while for C_δ it is $+4.7$ ppm ($\Delta\delta^{exp} = +4.8$ ppm). Finally, a large chemical shift difference of 72 ppm is observed experimentally for N_π, while no change occurs for N_τ. The theoretical results also show a large difference of 90 ppm for N_π, while N_τ is predicted to shift by 13 ppm. The ^{1}H signals are reproduced very well, both in absolute and relative values (see Tables 3.1 and 3.2).

Figure 3.4b presents the experimental chemical shift differences $\Delta\delta$ between α-His 37 andβ-His 12 (Table 3.2) compared with the theoretical $\Delta\delta$ between neutral$_\tau$ and neutral$_\tau$ including a hydrogen bonded water at the N_τ site (Table 3.1). This comparison reveals that the presence of a hydrogen bond affects mainly the N_τ chemical shift and confirms the experimental suggestion that β-His 12 is involved in a hydrogen bond. [26,39]

Mg-coordinated histidines (α-His 31, β-His 30)

The DFT results for various BChl *a*–His complex models are collected in Table 3.2. It has been suggested that these Mg-coordinated histidines may be involved in hydrogen bonding on the N_π side with the C13^1-keto carbonyl of the adjacent bacteriochlorophyll *a* molecule. [26,39] Therefore complexes **2**, **4** and **5** were studied, which include an inter-molecular hydrogen bond between N_π and a water molecule. The structure of the BChl *a*–His complexes **1** and **2** was fully optimized, while the complexes **3** and **4** were kept fixed according to the crystallographic data. [36] The complex **5** was partially optimized in the presence of some geometrical constraints, as explained below.

By comparing the chemical shifts for the complexes with and without the hydrogen bond, it is seen that the main effect is a change of 8 ppm in the chemical shift of the pyrrole-type nitrogen. Since this type of nitrogen gives a NMR resonance at 170 ppm, the observed chemical shift value of 178 ppm for N_π in Mg-coordinated histidine can be indeed attributed to the presence

of a hydrogen bond. However, a careful analysis of the X-ray structure in the vicinity of the β-His 30 leads to the conclusion that the hydrogen bond partner is the alanine β-Ala 26 and not the carbonyl group of the adjacent BChl *a* molecule suggested earlier. [26, 39]. Thus, the Ala 26 C=O forms two hydrogen bonds with His 30: one with the backbone NH and one with the side chain N_π. A similar situation occurs for the α-His 31 and α-Ala 27.

The computed chemical shifts for the imidazole protons H_δ and H_ε in the BChl *a*–His complexes (Table 3.2) clearly show a ring current effect of about 4 ppm when compared with the values for the non-coordinated histidines (Table 3.1), which is in very good agreement with the experiment.

The ^{13}C experimental data for the Mg-coordinated histidines are the same as those of the cationic histidine, suggesting that a charge transfer is taking place from the histidine to the bacteriochlorophyll. [26, 39] The DFT ^{13}C chemical shifts are in much better agreement with the experimental values when the X-ray structure is considered without performing a geometry optimization (Table 3.2, complexes **2** and **4**). This result pinpoints that the constraints due to the protein environment have a significant effect on the electronic structure of the BChl *a*–His complex. The comparison between the crystallographic data and the optimized geometry shows that in the course of geometry optimization (i) the Mg–N_τ distance increases from 2.12 Å to 2.31 Å in the DFT-optimized structure; (ii) the dihedral angle φ defined by N4, Mg, N_τ and C_ε, which represents the rotation of histidine around the Mg–N_τ axis, increases from 32° to 48°; and (iii) the BChl *a* ring becomes more flat. These changes in the geometry correspond to a change in the total imidazole ring charge from 0.2 for the optimized complex **2** to 0.5 for the non-optimized complex **4**, clarifying why the formally neutral$_\pi$ Mg-coordinated histidine in LH2 behaves as cationic histidine.

According to the X-ray data the imidazole ring of β-His 30 shows bond lengths typical for doubly protonated histidines. However, the RMSD on the bond lengths in the LH2 X-ray data is 0.03 Å, which is about the bond length difference between cationic and neutral$_\pi$ histidines. Therefore a constrained geometry optimization of the BChl *a*–His complex was additionally performed, in which only the imidazole ring was relaxed, while the Mg–N_τ

distance and the dihedral angle φ defined above were kept fixed. It was found that: (i) the charge transfer is essentially the same as obtained using the non-optimized crystal structure; (ii) a RMSD of 4.5 ppm for the ^{13}C chemical shifts resulting from this partially optimized structure is the same as for the crystal structure (see Table 3.2, complexes **4** and **5**); (iii) the bond lengths in the imidazole ring are now systematically shorter by 0.01–0.02 Å with respect to the fully optimized structure, as presented in Figure 3.5. It can be con-

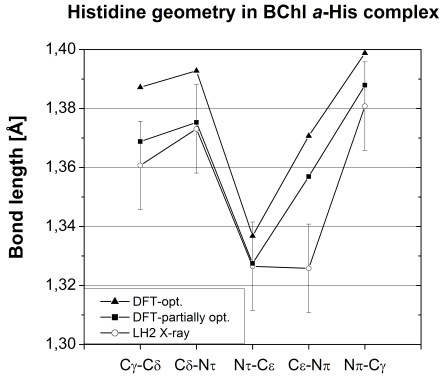

Figure 3.5: Bond lengths of the histidine imidazole ring in BChl *a*–His complex: DFT-optimized structure (triangles), DFT-partially optimized structure (squares) and X-ray structure of LH2 [36] (open circles).

cluded that the charge transfer depends crucially on the relative distance and orientation of the BChl *a*–His complex. This charge transfer can be clearly visualized by computing the charge density difference between the BChl *a*–His complex and the two fragments, His and BChl *a*, separately (Figure 3.6). The DFT results strongly suggest that the protein environment is forcing the histidine to stay close to the BChl *a*, thereby inducing a combined structural change and a large charge transfer. When the constraints from the protein are removed, the structure relaxes and histidine moves away from its close position to the bacteriochlorophyll *a*.

Although the ^{13}C data show the character of cationic histidine, the Mg-coordinated N_τ still maintains its pyridine character. [26] This is also con-

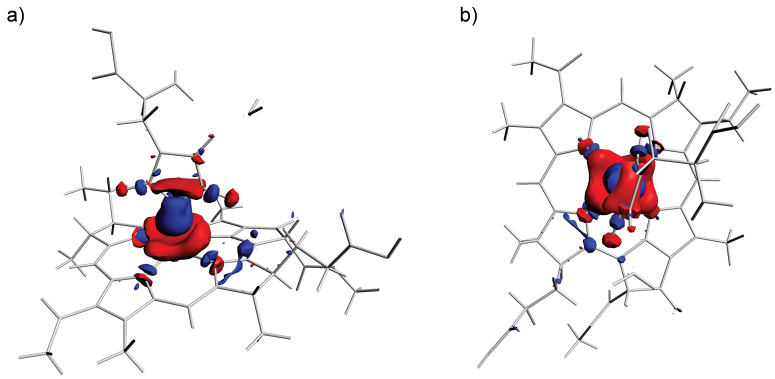

Figure 3.6: Change in the electronic density upon BChl *a*–His complex formation, calculated for the partially optimized structure (see text for details). The isosurface value is 0.0012 e/Å^3. Red corresponds to an increase of the density in the complex, as compared to the separated BChl *a* and His fragments, while blue denotes a decrease in the electronic density. a) Side view and b) top view.

firmed by the calculated anisotropy parameters for N_τ in the complex **5**: The computed δ and η are 8.9 kHz and 0.5, respectively, *vs.* 8.4 kHz and 0.4 estimated from NMR measurements [26] and agree well with the values expected for pyridine-type nitrogen. These results emphasize the state of frustration, especially for the N_τ and may indicate that histidine is in a protein-induced frustrated state between the neutral and the cationic electronic structure.

This finding of a protein induced charge transfer in the BChl *a*–His complex may have important effects on the absorption spectra and excitation energy transfer processes observed in LH2. Not only the excitation site energies and transition dipole moments of the BChl *a*–His complex, but also the long-range electrostatic interactions with the protein environment may change significantly. Preliminary time-dependent DFT calculations performed on the BChl *a*–His model and presented in Table 3.3 show a significant effect mainly on the Q_x absorption band when compared to the isolated BChl *a*. This result appears to be in line with absorption spectroscopy studies of BChl *a* in solvents. [101] In a recent DFT study, Neugebauer [102] has addressed the issue of the environmental effects on the excitation energies and photophysical properties of LH2 complexes. However, in that study the histidine has been

	Q_x			Q_y		
	E_{exc}	f	type	E_{exc}	f	type
BChl *a*	1.94	0.10	H-1 → L 83%	1.56	0.31	H → L 94%
BChl *a*–His	1.87	0.08	H-1 → L 85%	1.56	0.28	H → L 94%

Table 3.3: Calculated (SAOP/TZP) excitation energies (eV) and oscillatory strengths for BChl *a* and BChl *a*–His models. 'H' corresponds to HOMO and 'L' corresponds to LUMO.

modeled by a frozen density embedding approach, which may be inappropriate when charge transfer is taking place.

3.4 Conclusions

A comprehensive DFT analysis of the chemical shifts for different protonation states of the histidine imidazole ring was presented. The comparison with experimental data for crystal samples shows that trends can be predicted with good accuracy and that the largest errors are observed for pyridine type nitrogen atoms that may be strongly affected by the specific environment.

The DFT chemical shifts support the recently proposed assignment of the histidines protonation state in LH2 and confirm that all the histidines except α-His 37 participate in a hydrogen bond. Moreover, the results put forward the idea that the protein environment in LH2 exerts a stress on the Mg-coordinated histidines that induces a considerable electron charge transfer to the bacteriochlorophylls *a*, what explains why these histidines behave as cationic and not as neutral$_\pi$ histidines. This result has already stimulated more thorough investigation of protein local frustrations, with NMR chemical shifts used as markers. [103] The observed charge transfer may have far-reaching consequences on the absorption properties and photophysics of the BChl *a* macrocycle in the LH2 dimeric B850 complex. The understanding of these basic functional mechanisms will guide the design of future artificial photosynthesis devices.